Progress In Electromagnetics Research C, Vol. 105, 23–33, 2020

Study of Resistive Thin-Film Coatings for Application in Millimeter-Band Vacuum Power Amplifiers

Andrey V. Starodubov[1, 2, *], Stanislav A. Makarkin[1], Alexey A. Serdobintsev[1], Anton M. Pavlov[1], Victor V. Galushka[1], and Ilya O. Kozhevnikov[1]

Abstract—The aim of this work is to discuss the possibility of resistive thin-film coatings used for vacuum electron devices. Following a short review, results on radiophysical parameters studies in millimeter-band of such coatings are presented. Resistive Sn-O coatings with varied oxygen content were fabricated on quartz substrates by reactive magnetron sputtering. Morphology and elemental composition of prepared coatings were studied by means of scanning electron microscopy and secondary ion mass spectrometry, while four-probe method was utilized to study the resistivity of those. Dielectric properties were measured in the V-band (50–70 GHz) in free space using vector network analyzer. It was demonstrated that resistivity and the dielectric properties of coating in millimeter-band can be widely varied by controlling coating composition.

1. INTRODUCTION

Microwave signals amplification by vacuum electronic devices remains a spot of interest for many researchers with main focus gradually shifting towards shorter wavelengths — millimeter and submillimeter (terahertz) bands [1–5], which appear very promising for various modern applications such as broadband wireless communications, non-destructive evaluation, biomedical analyses, and radar systems [5–10]. Terahertz radiation can penetrate numerous dielectric and water-free materials that could be opaque for visible and mid-infrared light [11]; therefore, millimeter and THz waves are also promising for imaging applications and photodetection [12], including medical diagnostics, process control, and security [13]. One of the main challenges for the development of amplifiers in millimeter and submillimeter ranges is the fabrication of microsized slow-wave structures which is difficult to implement with conventional technologies. Various microfabrication methods are proposed instead, including lithography-based approaches (LIGA, UV-LIGA, deep reactive ion etching — DRIE), electric discharge machining (EDM), laser ablation, 3D-printing, micro- and nano- CNC-milling [14–20]. All of these technologies are quite expensive and labour-consuming.

In these circumstances, "forgotten" ideas on amplifying microwave signals with electron-wave and resistive wall amplifiers has recently drawn attention as a potential alternative approach [21–26].

Here authors aim to give a short review of the scientific background on the possibility of using resistive thin-film coatings to amplify microwave signals as well as consider fabrication and experimental study of tin oxide based resistive thin-film coating for millimeter-wave band (V-band) amplifiers. Extended reviews of resistive thin films coatings technology for microwave signals amplification can be found elsewhere [27–29]. Dielectric properties of the 0.5 mm thick quartz slides with resistive thin-film coatings were studied in the millimeter wavelength range (V-band, 50–70 GHz), which seems most promising from the point of view of the development of future 5th generation wireless communication systems (5G), as well as satellite communications and telecommunications [30, 31].

Received 16 April 2020, Accepted 6 August 2020, Scheduled 25 August 2020

* Corresponding author: Andrey V. Starodubov (StarodubovAV@gmail.com).

[1] Saratov State University, 83 Astrakhanskaya Street, Saratov 410012, Russia. [2] Micro- and Nanoelectronics Laboratory, Saratov Branch, V.A. Kotel'nikov Institute of Radio Engineering and Electronics RAS, 38 Zelyonaya st., Saratov 410019, Russia.

2. RESISTIVE WALL AMPLIFIER CONCEPT DEVELOPMENT

The idea of a resistive wall amplifier (RWA) was initially proposed [22, 24, 25]. In this device, the electron beam is guided along a wall with conductive losses to amplify a microwave signal. Passing the electron beam near a resistive medium induces charges in the wall and the space charge forces associated with the wall charges to act on the electron stream causing electron bunches to form as the electron beam propagates. This bunching of the electron beam results in an exponential growth of longitudinal electron beam current AC component. A principal scheme of resistive wall amplifier is presented in Fig. 1. In contrast to the traveling-wave devices, there is essentially no interaction between the signal carrying electromagnetic wave and the electron beam. This allows for the replacement of a conventional slow-wave structure such as helix with a resistive thin-film coating. Although some energy is dissipated due to ohmic losses, there is a finite rate of growth for all stream currents. Several experimental studies were carried out. In these experiments, the laboratory setup consisted of a cylindrical electron stream guiding coaxial glass tube (dielectric support) coated on the inside with a resistive material. The thickness of the glass tube walls was about 130 μm, and the resistive coating of tin oxide on the inner surface was deposited onto the hot glass from stannous chloride vapor. Capability of RWA to perform as a high-gain broadband amplifier was demonstrated [24].

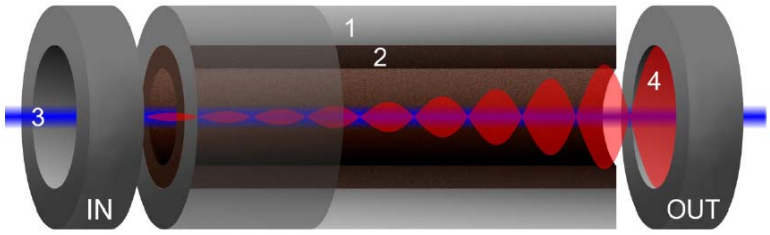

Figure 1. Resistive wall amplifier schematic: 1 — support material (dielectric), 2 — thin-film resistive layer, 3 — electron stream, 4 — space-charge wave, "IN" — input circuit, "OUT" — output circuit.

However, it was found that limitations of physical implementation feasibility of the device result in a substantial reduction of RWAs parameters. Particularly, the gain of the device depends on the type of wall admittance at the edge of the electron beam [24, 25]. In the cases of perfectly conducting and dielectric walls, as well as walls with a capacitive load, no signal gain is achieved. Pure inductive admittances provide the highest device gains. The capacitive portion of the admittance seen at the edge of the beam is increased with the dielectric constant of the material used to support the resistive medium and decrease of the beam filling factor together with the device gain. Large gain values are achievable only when the support material of the resistive wall is thin and has a very low dielectric constant [24, 25]. An ideal device would consist of a self-standing resistive layer surrounding electrons beam which is much thinner than skin layer [24]. As this cannot be accomplished in practice, dielectric substrates are introduced, which are kept as thin as possible to minimize capacitive-stunting effect. Particularly, a glass tube with 5 mil thick walls was utilized [24, 25]. Furthermore, gain maximization requires the edge of the electron beam to be very close to the resistive wall, which is difficult to implement in practice [24, 25]. Measured gain turned out to be smaller than the theoretical due to some of the above-mentioned factors (the presence of active and capacitive resistance in the device), about 20 dB in 1–4 GHz. The beam current was up to 20 mA, and accelerating voltage was 300–1000 V. The tube was operated with a magnetic field about 800 gauss, which approximately corresponded to the characteristics of the traveling-wave tube. Also, the device had a fairly high noise level. However, this rather simple design had a gain and bandwidth comparable to a helix-type traveling wave tube. The signal input is effectively isolated from the output by a lossy circuit so that parasitic oscillations due to internal feedback are inherently absent. Amplifier gain was weakly dependent on the average electron flow velocity which is explained by the fact that the operation of this device is not based on the principle of synchronism of the electron flow with a phase velocity of the electromagnetic wave in the system, but on the use of the phase shift between the convection current and the electric field strength due to the conductivity of the resistive wall. Resistive wall amplifier had a great potential in millimeter

and submillimeter wavelength range using because it was not necessary to microfabricate slow-wave structures with extremely small elements.

As mentioned above, the greatest gain was achieved with a purely inductive impedance of the walls of the RWA (or simply with an inductive component of the resistance, far superior to the rest). This is very similar to the easitron proposed by Pierce and manufactured by Walker in the 3 cm wavelength range [32]. This device was a rectangular waveguide, partially filled with a dielectric, in which the electrodynamics system used was a set of half-wave wires drawn between the sidewalls of the waveguide, representing a set of resonator elements. The equivalent circuit of such an electrodynamics system looks like a standard long line with no losses, but with negative capacitances. As shown by Pierce, when electrons flow passes through an inductively or resistively conductive medium, growing and decaying space charge waves can appear. Another group of scientists came up with a similar model that uses elements in the waveguide that create inductive resistance [27]. Theoretical investigations and numerical calculations were performed for a high-frequency resistive wall klystron, in which a relativistic electron beam was modulated at the first cavity and propagated downstream through a resistive wall [33–35]. It was shown that due to self-excitation of the space charge waves by the resistive-wall instability, a highly nonlinear current modulation is accomplished. As the instability increases relatively quickly, the required tube length of the klystron is short for most applications.

Recently, the concept of a metamaterial-enhanced RWA (ME-RWA) was proposed [27]. In this device, metamaterials have replaced both the resistive and support materials used in the conventional RWA. Epsilon-negative metamaterials were utilized as metamaterials to provide the necessary effective inductive admittance for the beam, to achieve amplification with near-theoretical gain values. Results of a metamaterial structure simulation that can be used to construct a metamaterial-enhanced RWA were presented [29]. It was demonstrated that a periodic arrangement of inductive meandered lines can be used as a practical metal-based epsilon negative metamaterial implementation with a Drude-Lorentz type permittivity. The results of the numerical study of dispersion and gain of the ME-RWA structure were presented. Experimental study of the proposed structure was also carried out [36]. Metamaterial (MTM)-inspired vacuum electron devices have several significant advantages, such as small size, high power, high efficiency, and high gain (review of this topic in [37, 38]). Several results of experimental studies in GHz range of high power (> 1 MW) [38] microwave devices with MTM structures were observed, but it was noted that the major difficulty is the fabrication of such materials due to their subwavelength structure.

Thus, although resistive coatings seem an adequate alternative to classical slowing systems in mm and sub-mm ranges, only one successful experiment on resistive wall amplifier construction was reported for GHz band [24]. Main characteristics of a resistive amplifier (including gain factor) are governed by electrical parameters (conductivity, complex dielectric properties) of coatings, which, in turn, are determined by chemical composition of materials being used [24, 25, 27, 28]. Thus, the right choice of materials is a key for successful implementation of such devices. Results of investigations on structural properties, conductivity, and dielectric properties of resistive coatings in mm band depending on chemical composition are presented here. Sn-O elemental system was studied following the initial reports [24, 25], and reactive magnetron sputtering was utilized to prepare resistive coatings with controlled elemental composition.

3. FABRICATION OF RESISTIVE THIN-FILM COATINGS

Several samples of coatings were prepared by magnetron sputtering with varied composition (Sn:O ratio) upon 0.5 mm thick 60×60 mm quartz slides. The choice of quartz as a substrate was governed by its low dielectric constant of ~ 3.7. Deposition was performed using NexDep magnetron sputtering unit (Angstrom Engineering, Canada) with oil-free pumping and 99.999% pure 76 mm tin target (Girmet, Russia). The base pressure in the working chamber did not exceed $2 \cdot 10^{-5}$ Torr, with deposition pressure regulated at $5 \cdot 10^{-3}$ Torr. Amount of oxygen in the working gas mixture was the varied parameter to control the chemical composition of the coatings. Each sample was prepared in triplicate. Description of the samples is presented in Table 1. A photo of fabricated samples is presented in Fig. 2. It can be seen that as the amount of oxygen in the working gas mixture increases, coatings acquire mirror properties (at 50% oxygen, the coating almost resembles a good mirror).

Table 1. Samples description.

Sample	Oxygen portion in working gas mixture, %	Coating thickness, nm	Coating resistivity, Ω·cm
1	0	1075 ± 75	0.048 ± 0.002
2	17	1100 ± 70	2.5 ± 0.6
3	29	1200 ± 20	36.0 ± 0.4
4	38	1070 ± 10	64 ± 6
5	50	970 ± 6	13200 ± 547

Figure 2. Photo of fabricated samples of resistive thin-film coatings with different oxygen content in the gas mixture in the process of magnetron sputtering on 60×60 mm quartz slides. Samples numbering corresponds to Table 1.

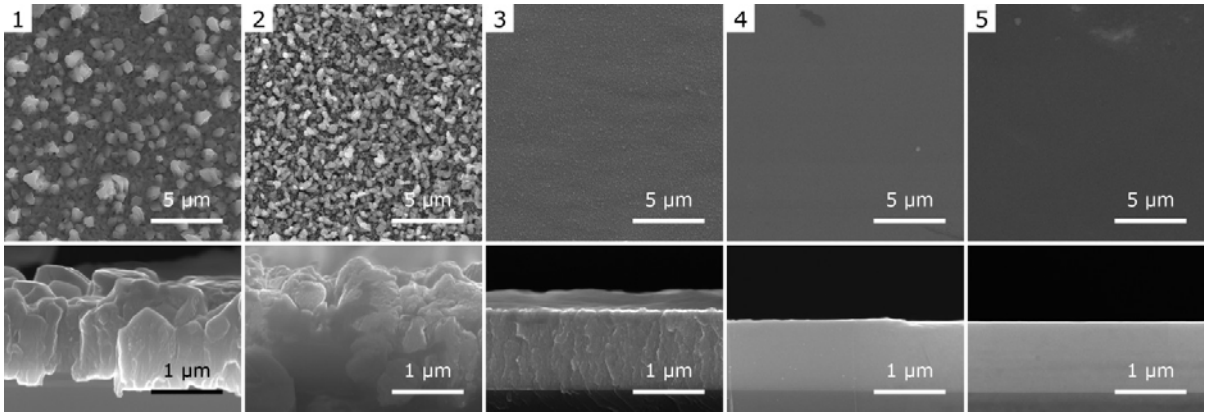

Figure 3. SEM images of films surface (top row) and witness samples (cleaved monocrystalline silicon, side view, bottom row).

In order to control the thickness of the prepared coatings, a witness sample (a piece of monocrystalline silicon) was placed near the quartz slides upon sputtering, whose cleaved facets were then visualized by scanning electron microscopy (SEM) using Tescan MIRA II scanning electron microscope (see Fig. 3). It was found that as the amount of oxygen in the working gas mixture increases, the coating becomes thinner, denser, and more uniform. This can be attributed to the decrease of crystallites size in coatings as oxygen content increases. Large crystallites (larger than coating thickness) are characteristic for pristine metal. This results in pronounced surface roughness and higher measured thickness values (samples #1 and #2, Fig. 3) which decreases in coatings with

higher oxygen content (samples #3 and #4, Fig. 3) as film gains solid structure and crystallite inclusions become nano-sized and evenly formed. As oxygen content becomes even higher (sample #5, Fig. 3), the film becomes dense and fully continuous with very low surface roughness. Low roughness of samples with higher oxygen content also results in mirror glare of the surface of those. These effects might be attributed to the change of microcrystalline film structure to nanocrystalline or even amorphous, which obviously needs further confirmation and is out of scope of this report.

The change of oxygen content in deposited coatings was confirmed by results of energy dispersive X-ray analysis (EDX analysis), which indicate the increase of oxygen content in the coatings with oxygen portion in the working gas mixture during magnetron sputtering process (Fig. 4(a)). Oxygen presence in coating with zero oxygen content in working gas mixture (sample #1) can be attributed to a natural surface oxidation of the coating in the atmosphere which is promoted by elevated film roughness resulting in high exposed surface area.

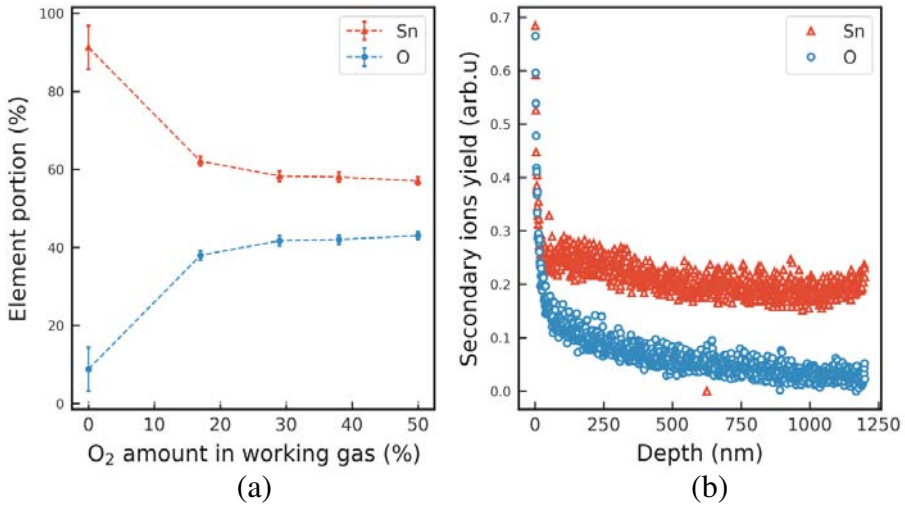

Figure 4. Elemental composition of resistive coatings. A — results of EDX analysis, B — a typical SIMS ion etching profile of oxygen and tin ions (results for sample #3 are presented).

Secondary ion mass spectrometry (SIMS) studies were carried out using PHI 4300 spectrometer (Perkin-Elmer, USA). The setup is equipped with a sector electrostatic filter and a quadrupole mass analyzer. Sputtering was performed with argon ions with acceleration voltage of 4 kV and the current of the primary ions of 1 μA. To increase the depth resolution and eliminate the crater effect, the primary ion beam scanned a 4×4 mm sample area. At the same time, the beam of secondary ions passed through electrostatic diaphragms, which cut off secondary ions emerging from the walls of the sputtering crater. As a result, nanometer-scale depth resolution was achieved. The secondary ions of the most abundant isotopes ^{120}Sn and ^{16}O were recorded. The profiles of ions distribution across the coating thickness for all samples were obtained in order to study the homogeneity of elemental composition.

Tin and oxygen profiles were almost identical for all samples, except sample #1. Characteristic graphs are presented in Fig. 4(b). For the convenience of comparison, the signals of secondary ions of tin and oxygen were normalized. A disturbed surface layer is present on the surface of the coating, which results in a high level of secondary ions yield, both oxygen and tin, at the initial moment of sputtering, followed by a sharp drop in the output level, corresponding to the removal of the disturbed surface layer. Further, the signal of secondary ions corresponds to the true content of tin and oxygen in the volume of the coatings studied. In this case, the yield of secondary ions of both elements stays almost constant during the sputtering process, which indicates the uniformity of elemental composition over the entire thickness of the coating.

4. RESULTS OF EXPERIMENTAL STUDY OF ELECTRICAL PROPERTIES

Resistivity of obtained coatings was measured by two methods: the four-probe method using Tektronix PWS2326 stabilized power supply unit, a F195 microammeter, a FLUKE 27II multimeter, and a laboratory setup of tungsten probes located in line with a 2 mm gaps were used. The voltage from power supply was applied to the external probes. Current through external probes and the voltage at the internal ones were recorded. The results of resistivity studies presented in Fig. 5 demonstrate increase of the resistivity with oxygen content in the film (calculated from EDX data, see Fig. 4(a)). This result seems consistent since an increase of oxygen content leads to the oxidation of a larger number of tin atoms which results in the resistivity increase if the resulting films.

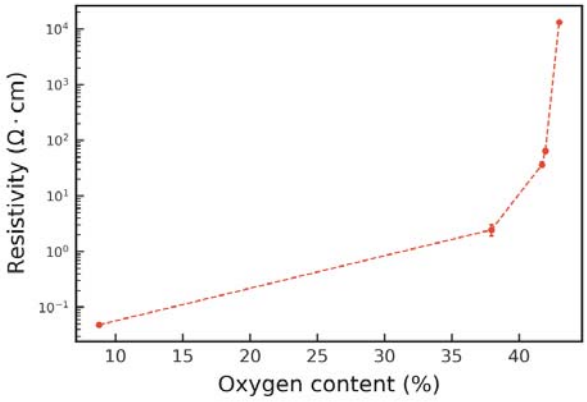

Figure 5. Results of the resistivity studies of resistive coatings with different oxygen content (from EDX data, see Fig. 4(a)).

Using frequency dependent model of sheet resistance of conductive coatings proposed by Liu and Tan [39] it is possible to calculate the resistance or conductivity at millimeter and terahertz frequencies based on measured DC resistivity values:

$$R_{\text{coat}} = \frac{1}{\sigma\delta\left(1 - e^{-\frac{t}{\delta}}\right)},$$

where σ is the DC conductivity, t the thickness of the coating, and the skin depth δ can be calculated as:

$$\delta = \sqrt{\frac{1}{\pi f \mu_0 \sigma}}$$

where f is the frequency, and $\mu_0 = 4\pi \cdot 10^{-7}$ H/m is the permeability of vacuum.

Effective conductivity at millimeter and terahertz frequencies is known to depend strongly in some cases on the surface roughness [40]. Based on the calculation by Morgan [41] of the reflection loss of a plane wave due to reflection from a grooved metal surface E. O. Hammerstad and F. Bekkadal suggested the model for effective conductivity σ_{eff} calculation, which depends only on the surface root mean square (RMS) roughness R_s and skin depth δ [42]:

$$\sigma_{eff} = \frac{\sigma}{\left(1 + \frac{2}{\pi}\tan^{-1}\left(1.4\left(\frac{R_s}{\delta}\right)^2\right)\right)^2}.$$

Experimental study of dielectric parameters of the quartz slides coated with resistive coatings of various compositions was carried out in free space [43–45], using a Keysight Technologies PNA N5227A vector network analyzer, two V-band horn antennas (ARH-1520-01, Ducommun Technologies Inc) precisely mounted on optical rails together with sample holders presented in Fig. 6.

Figure 6. Experimental setup for dielectric parameters measurement in free space with N5227A vector network analyzer, two V-band horn antennas and a tested sample between these assembled on optical rails.

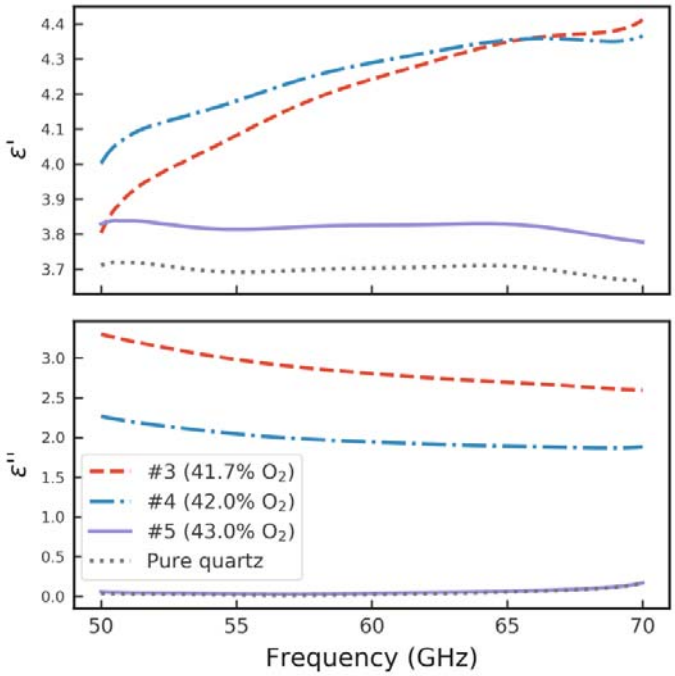

Figure 7. Measured real and imaginary parts of the complex dielectric constant of quartz slides coated with resistive coatings with different oxygen content (from EDX data, see Fig. 4(a)). Measurements results of pure slides are provided for comparison.

The test sample was placed in the middle between the antenna horns. On waveguide connectors of horn antennas, a full two-port TRL (Thru-Reflect-Line) type calibration was performed using a mechanical calibration kit. Then, in order to reduce measurement errors due to diffraction effects at the borders of the sample and multiple residual reflections between antennas, the GRL (Gated-Reflect-Line) type calibration was performed using time-domain measurements. The GRL calibration method converts a 2-port calibration of measurements using a coaxial line or waveguide into a full

2-port calibration in free space. After performing the above-mentioned calibration procedures, the S-parameters of the sample under study were measured. Obtained results show the increase of S_{11} and decrease of S_{21} with the increase of oxygen content in the coating. At oxygen content of 50% in the working gas mixture during magnetron sputtering deposited resistive coating introduces no changes to the clear quartz slide parameters. The dielectric constants were calculated using the Keysight Technologies N1500A Materials Measurement Suite software [46] from the measured S-parameters. The dependences of the dielectric constants of the samples on the frequency for different variations of the coating composition are presented in Fig. 7. It was found that by varying the composition of the coating, it is possible to control the dielectric constant in rather wide range from the properties of an almost conducting material to the properties of a complete dielectric. The dielectric properties of samples #1 and #2 are absent in Fig. 7 due to very their high conductivity, comparable to that of a metal plate used as the equivalent of full reflection during the free space calibration procedure which results in complex dielectric constant values calculated from measured S-parameters falling outside the range of values valid for permittivity evaluation algorithms of Keysight Technologies N1500A Materials Measurement Suite software.

5. CONCLUSIONS

In this work, we consider a short review of resistive coatings and its further development as metamaterials layers as a possible alternative to a conventional slow-wave structure in vacuum electron devices. The different compositions of resistive film coatings based tine oxide were fabricated on quartz substrates using the magnetron sputtering approach. The results of SEM and SIMS study of different compositions of resistive film coatings were considered. We carried out the study of properties of resistive film coatings based on tine oxide in the millimeter band (V-band). Analysis of S-parameters and dielectric constants of quartz substrates with deposited resistive thin-film coatings has shown that by varying the oxygen content in the working gas mixture during the magnetron sputtering process, it is possible to control the properties of coatings.

In future work, we are going to consider an alternative basis for a resistive thin-film coating such as silicon-tungsten. Such materials have significantly greater chemical resistance, resistance to thermal loads, high thermal stress, etc. The latter is especially important for devices of vacuum microwave electronics, in which the operation of thermal cathodes has a significant thermal effect on all internal elements of the electron-optical system, the drift space and the collector region, and energy input and output elements. It should be noticed that the presented results of the study are also meaningful and useful not only for the RWA development but also for a number of applications and microwave techniques involving high-loss materials including absorbing dielectrics [47–51].

ACKNOWLEDGMENT

This work was supported by 18-32-00937 mol_a research grant of Russian Foundation for Basic Research (RFBR).

REFERENCES

1. Siegel, P. H., "Terahertz technology," *IEEE Trans. Microw. Theory Tech.*, Vol. 50, No. 3, 910–928, Mar. 2002, doi: 10.1109/22.989974.
2. Sherwin, M., "Terahertz power," *Nature*, Vol. 420, No. 6912, 131–133, Nov. 2002, doi: 10.1038/420131a.
3. Booske, J. H., et al., "Vacuum electronic high power terahertz sources," *IEEE Trans. Terahertz Sci. Technol.*, Vol. 1, No. 1, 54–75, Sep. 2011, doi: 10.1109/TTHZ.2011.2151610.
4. Lewis, R. A., "A review of terahertz sources," *J. Phys. D: Appl. Phys.*, Vol. 47, No. 37, 374001, Sep. 2014, doi: 10.1088/0022-3727/47/37/374001.
5. Bratman, V. L., A. G. Litvak, and E. V. Suvorov, "Mastering the terahertz domain: Sources and applications," *Uspekhi Fiz. Nauk*, Vol. 181, No. 8, 867, 2011, doi: 10.3367/UFNr.0181.201108f.0867.

6. Fan, S., Y. He, B. S. Ung, and E. Pickwell-MacPherson, "The growth of biomedical terahertz research," *J. Phys. D: Appl. Phys.*, Vol. 47, No. 37, 374009, Sep. 2014, doi: 10.1088/0022-3727/47/37/374009.
7. Linfield, E., "A source of fresh hope," *Nat. Photonics*, Vol. 1, No. 5, 257–258, May 2007, doi: 10.1038/nphoton.2007.56.
8. Tonouchi, M., "Cutting-edge terahertz technology," *Nat. Photonics*, Vol. 1, No. 2, 97–105, Feb. 2007, doi: 10.1038/nphoton.2007.3.
9. Mukherjee, P. and B. Gupta, "Terahertz (THz) frequency sources and antennas — A brief review," *Int. J. Infrared Millimeter Waves*, Vol. 29, No. 12, 1091–1102, Dec. 2008, doi: 10.1007/s10762-008-9423-0.
10. Armstrong, C. M., "The truth about terahertz," *IEEE Spectr.*, Vol. 49, No. 9, 36–41, Sep. 2012, doi: 10.1109/MSPEC.2012.6281131.
11. Viti, L., A. Politano, and M. S. Vitiello, "Black phosphorus nanodevices at terahertz frequencies: Photodetectors and future challenges," *APL Mater.*, Vol. 5, No. 3, 2017, doi: 10.1063/1.4979090.
12. Viti, L., et al., "Plasma-wave terahertz detection mediated by topological insulators surface states," *Nano Lett.*, Vol. 16, No. 1, 80–87, 2016, doi: 10.1021/acs.nanolett.5b02901.
13. Vicarelli, L., et al., "Graphene field-effect transistors as room-temperature terahertz detectors," *Nat. Mater.*, Vol. 11, No. 10, 865–871, 2012, doi: 10.1038/nmat3417.
14. Joye, C. D., J. P. Calame, M. Garven, and B. Levush, "UV-LIGA microfabrication of 220 GHz sheet beam amplifier gratings with SU-8 photoresists," *J. Micromechanics Microengineering*, Vol. 20, No. 12, 125016, Dec. 2010, doi: 10.1088/0960-1317/20/12/125016.
15. Gamzina, D., et al., "Nano-CNC machining of sub-THz vacuum electron devices," *IEEE Trans. Electron Devices*, Vol. 63, No. 10, 4067–4073, Oct. 2016, doi: 10.1109/TED.2016.2594027.
16. Ryskin, N. M., et al., "Planar microstrip slow-wave structure for low-voltage V-band traveling-wave tube with a sheet electron beam," *IEEE Electron Device Lett.*, Vol. 39, No. 5, 757–760, May 2018, doi: 10.1109/LED.2018.2821770.
17. Starodubov, A. V., et al., "Planar slow-wave structures for low-voltage millimeter-band vacuum devices (Novel approach for fabrication, numerical and experimental measurements)," *2018 18th Mediterranean Microwave Symposium (MMS)*, 128–131, Oct. 2018, doi: 10.1109/MMS.2018.8612075.
18. Starodubov, A. V., A. A. Serdobintsev, A. M. Pavlov, V. V. Galushka, P. V. Ryabukho, and N. M. Ryskin, "A novel approach to microfabrication of planar microstrip meander-line slow wave structures for millimeter-band TWT," *2018 Progress In Electromagnetics Research Symposium (PIERS — Toyama)*, 506–509, Japan, Aug. 1–4, 2018.
19. Cook, A. M., C. D. Joye, and J. P. Calame, "W-band and D-band traveling-wave tube circuits fabricated by 3D printing," *IEEE Access*, Vol. 7, 72561–72566, 2019, doi: 10.1109/ACCESS.2019.2920291.
20. Baik, C.-W., et al., "Dispersion retrieval from multi-level ultra-deep reactive-ion-etched microstructures for terahertz slow-wave circuits," *Appl. Phys. Lett.*, Vol. 104, No. 2, 021118, Jan. 2014, doi: 10.1063/1.4862324.
21. Haeff, A. V., "The electron-wave tube — A novel method of generation and amplification of microwave energy," *Proc. IRE*, Vol. 37, No. 1, 4–10, Jan. 1949, doi: 10.1109/JRPROC.1949.232968.
22. Pierce, J. R., "Waves in electron streams and circuits," *Bell Syst. Tech. J.*, Vol. 30, No. 3, 626–651, Jul. 1951, doi: 10.1002/j.1538-7305.1951.tb03672.x.
23. Kalinin, Y. A. and A. V. Starodubov, "Study of electron-wave microwave amplifiers at high values of the inhomogeneity parameters of the electron beam velocities," *Radiophys. Quantum Electron.*, Vol. 62, No. 1, 26–32, Jun. 2019, doi: 10.1007/s11141-019-09951-4.
24. Birdsall, C., G. Brewer, and A. Haeff, "The resistive-wall amplifier," *Proc. IRE*, Vol. 41, No. 7, 865–875, Jul. 1953, doi: 10.1109/JRPROC.1953.274425.
25. Birdsall, C. K. and J. R. Whinnery, "Waves in an electron stream with general admittance walls," *J. Appl. Phys.*, Vol. 24, No. 3, 314–323, Mar. 1953, doi: 10.1063/1.1721272.

26. Lopukhin, V. M. and A. A. Vedenov, "The absorption amplifier," *Uspekhi Fiz. Nauk*, Vol. 53, No. 5, 69–86, 1954, doi: 10.3367/UFNr.0053.195405c.0069.
27. Rowe, T., J. H. Booske, and N. Behdad, "Metamaterial-enhanced resistive wall amplifiers: Theory and particle-in-cell simulations," *IEEE Trans. Plasma Sci.*, Vol. 43, No. 7, 2123–2131, Jul. 2015, doi: 10.1109/TPS.2015.2439159.
28. Starodubov, A., et al., "Resistive thin-film coatings as an alternative to classical slow wave structures in millimeter-wave vacuum electron devices," *Saratov Fall Meeting 2018: Laser Physics, Photonic Technologies, and Molecular Modeling*, 54, Jun. 2019, doi: 10.1117/12.2525059.
29. Rowe, T., N. Behdad, and J. H. Booske, "Metamaterial-enhanced resistive wall amplifier design using periodically spaced inductive meandered lines," *IEEE Trans. Plasma Sci.*, Vol. 44, No. 10, 2476–2484, Oct. 2016, doi: 10.1109/TPS.2016.2599144.
30. Lota, J., S. Sun, T. S. Rappaport, and A. Demosthenous, "5G uniform linear arrays with beamforming and spatial multiplexing at 28, 37, 64, and 71 GHz for outdoor urban communication: A two-level approach," *IEEE Trans. Veh. Technol.*, Vol. 66, No. 11, 9972–9985, Nov. 2017, doi: 10.1109/TVT.2017.2741260.
31. Niu, Y., Y. Li, D. Jin, L. Su, and A. V. Vasilakos, "A survey of millimeter wave communications (mmWave) for 5G: Opportunities and challenges," *Wirel. Networks*, Vol. 21, No. 8, 2657–2676, Nov. 2015, doi: 10.1007/s11276-015-0942-z.
32. Pierce, J. R., "The wave picture of microwave tubes," *Bell Syst. Tech. J.*, Vol. 33, No. 6, 1343–1372, Nov. 1954, doi: 10.1002/j.1538-7305.1954.tb03757.x.
33. Uhm, H. S., "Resistive-wall klystron," *Phys. Lett. A*, Vol. 182, No. 1, 120–124, Nov. 1993, doi: 10.1016/0375-9601(93)90064-7.
34. Uhm, H. S., "A self-consistent nonlinear theory of resistive-wall instability in a relativistic electron beam," *Phys. Plasmas*, Vol. 1, No. 6, 2038–2052, Jun. 1994, doi: 10.1063/1.870658.
35. Uhm, H. S., "The resistive-wall klystron as a high-power microwave source," *Proceedings Particle Accelerator Conference*, Vol. 3, 1527–1529, 1995, doi: 10.1109/PAC.1995.505274.
36. Rowe, T., P. Forbes, J. H. Booske, and N. Behdad, "Inductive meandered metal line metamaterial for rectangular waveguide linings," *IEEE Trans. Plasma Sci.*, Vol. 45, No. 4, 654–664, Apr. 2017, doi: 10.1109/TPS.2017.2675706.
37. Duan, Z., et al., "Review of metamaterial-inspired vacuum electron devices," *2018 IEEE International Vacuum Electronics Conference (IVEC)*, Vol. 8, 29–30, Apr. 2018, doi: 10.1109/IVEC.2018.8391536.
38. Duan, Z., et al., "Metamaterial-inspired vacuum electron devices and accelerators," *IEEE Trans. Electron Devices*, Vol. 66, No. 1, 207–218, Jan. 2019, doi: 10.1109/TED.2018.2878242.
39. Liu, Y. and J. Tan, "Frequency dependent model of sheet resistance and effect analysis on shielding effectiveness of transparent conductive mesh coatings," *Progress In Electromagnetics Research*, Vol. 140, 353–368, 2013.
40. Hu, P., et al., "Development of a 0.32-THz folded waveguide traveling wave tube," *IEEE Trans. Electron Devices*, Vol. 65, No. 6, 2164–2169, Jun. 2018, doi: 10.1109/TED.2017.2787682.
41. Morgan, S. P., "Effect of surface roughness on eddy current losses at microwave frequencies," *J. Appl. Phys.*, Vol. 20, No. 4, 352–362, Apr. 1949, doi: 10.1063/1.1698368.
42. Hammerstad, E. O. and F. Bekkadal, *Microstrip Handbook, ELAB report*, Trondheim: Norwegian Institute of Technology, 1975.
43. Beker-Jarvis, J., et al., "Measuring the permittivity and permebility of lossy materials: Solids, liquids, metals, building material, and negative-index materials," *NIST Tech. Note 1536*, 1–5, 2005, [online], available: http://nvlpubs.nist.gov/nistpubs/Legacy/TN/nbstechnicalnote1536.pdf.
44. Baker-Jarvis, J., E. J. Vanzura, and W. A. Kissick, "Improved technique for determining complex permittivity with the transmission/reflection method," *IEEE Trans. Microw. Theory Tech.*, Vol. 38, No. 8, 1096–1103, Aug. 1990, doi: 10.1109/22.57336.
45. Ghodgaonkar, D. K., V. V. Varadan, and V. K. Varadan, "Free-space measurement of complex permittivity and complex permeability of magnetic materials at microwave frequencies," *IEEE*

Trans. Instrum. Meas., Vol. 39, No. 2, 387–394, Apr. 1990, doi: 10.1109/19.52520.

46. Technologies, K., "Keysight technologies materials measurement?: Dielectric materials," 2018, [online], available: http://literature.cdn.keysight.com/litweb/pdf/5992-0263EN.pdf.
47. Loudon, R., "The propagation of electromagnetic energy through an absorbing dielectric," *J. Phys. A Gen. Phys.*, Vol. 3, No. 3, 233–245, May 1970, doi: 10.1088/0305-4470/3/3/008.
48. Chung, B.-K. and H.-T. Chuah, "Modeling of RF absorber for application in the design of anechoic chamber," *Progress In Electromagnetics Research*, Vol. 43, 273–285, 2003.
49. Ramprecht, J., M. Norgren, and D. Sjoberg, "Scattering from a thin magnetic layer with a periodic lateral magnetization: Application to electromagnetic absorbers," *Progress In Electromagnetics Research*, Vol. 83, 199–224, 2008.
50. Koledintseva, M. Y., A. G. Razmadze, A. Y. Gafarov, V. V. Khilkevich, J. L. Drewniak, and T. Tsutaoka, "Attenuation in extended structures coated with thin magneto-dielectric absorber layer," *Progress In Electromagnetics Research*, Vol. 118, 441–459, 2011.
51. Zhou, M., F. Lu, B. Liu, J. Yang, and X. Zeng, "Electrospun SnO_2 submicron fibers for broadband microwave absorption," *J. Phys. D. Appl. Phys.*, Vol. 48, No. 49, 495303, Dec. 2015, doi: 10.1088/0022-3727/48/49/495303.